

Directivity Effects of Shaped Plumes from Plug Nozzles

James D. Chase¹ and G. Andres Garzón²
Aerion Corporation, Reno NV 89502

and

D. Papamoschou³
University of California, Irvine CA 92697

A set of various shaped nozzles designed by Aerion Corporation were investigated on a reduced scale facility at University of California Irvine (UCI). Initial results on some of the configurations show great potential in directing the noise away from the relevant azimuth positions and producing significant reduction in noise levels. Flow surveys and numerical analysis have been performed to better understand the mechanisms which produce such improvement.

Nomenclature

D	=	Equivalent diameter
NPR	=	Nozzle Pressure Ratio
U	=	Mean axial velocity
U_e	=	Jet exit velocity for perfect expansion
θ	=	polar angle, measured from downstream axis
ρ	=	Local density from CFD
ρ_{inf}	=	Freestream density
ϕ	=	azimuthal angle, measured from downward vertical

I. Introduction

NOISE reduction in jet aircraft has become one of the most prolific areas of research. Attaining acceptable takeoff noise levels for supersonic aircraft is particularly challenging as they typically require engine cycles of significantly lower bypass ratios than current subsonic aircraft for efficient cruise. This results in high jet velocities at takeoff conditions that dominate noise emissions. Different mechanisms for reducing noise or redirecting it have been proposed and studied. Modifications to the shape of the jet plume have been studied by numerous authors, and have shown in general terms good results in directing the noise on specific directions. Jet plumes with elongated cross sections have shown a reduction on the noise in the direction of the longer axis, and modest increases in noise in the direction of the shorter axis¹. In their stability analysis of elliptic jets, Morris and Bhat² concluded that the unsteady structure in a naturally excited elliptic jet is expected to be dominated by the flapping mode. At high jet velocity this mode becomes supersonic and radiates very efficiently along the minor axis plane.

Aerion's supersonic business jet (SBJ) design uses a Pratt & Whitney JT8D engine with a medium bypass ratio of 1.8. This engine choice is a good match for supersonic operation at high altitude, but presents a challenge for noise at take off. As part of the design process of a supersonic business jet different nozzle configurations have been designed at Aerion Corporation and tested at UC Irvine's acoustic test facility.

¹ Chief Engineer, 1325 Airmotive Way Suite 370. Reno, NV 89502

² Manager Computational Aerodynamics, agarzon@aerioncorp.com, AIAA Senior Member.

³ Professor, Department of Mechanical and Aerospace Engineering, dpapamos@uci.edu, Fellow AIAA.

II. Test Facility

Noise measurements were performed in the aeroacoustic facility shown in Figure 1. The facility uses helium-air mixtures to simulate noise of hot jets³. The microphone array consisted of eight 3.2-mm condenser microphones (Bruel & Kjaer, Model 4138) arranged on a circular arc centered at the vicinity of the nozzle exit. The polar aperture of the array was 30° and the array radius was 1 m. The angular spacing of the microphones was logarithmic. The entire array structure was rotated around its center to place the array at the desired polar angle. Positioning of the array was done remotely using a stepper motor. An electronic inclinometer displays the position of first microphone. The arrangement of the microphones inside the anechoic chamber, and the principal electronic components, are shown in Figure 1. The microphones were connected, in groups of four, to two amplifier/signal conditioners (Bruel & Kjaer, Model 4138) with high-pass filter set at 300 Hz and low-pass filter set at 100 kHz. The four-channel output of each amplifier was sampled at 250 kHz per channel by a multi-function data acquisition board (National Instruments PCI-6070E). Two such boards, one for each amplifier, were installed in a Pentium 4 personal computer. National Instruments LabView software was used to acquire the signals. Even though the array provides noise source location maps, in this study it was used only to survey the far-field sound emitted by the jets. The sound pressure level spectrum was corrected for actuator response, free-field correction, and atmospheric absorption. The overall sound pressure level (OASPL) was obtained by integrating the corrected spectrum. Spectra and OASPL are referenced to a distance of 100 nozzle exit diameters from the nozzle exit. Measurement at different azimuthal planes was possible by rotating the nozzle. The azimuth angle ϕ , relevant for the non-axisymmetric configurations, is measured from the downward vertical direction.

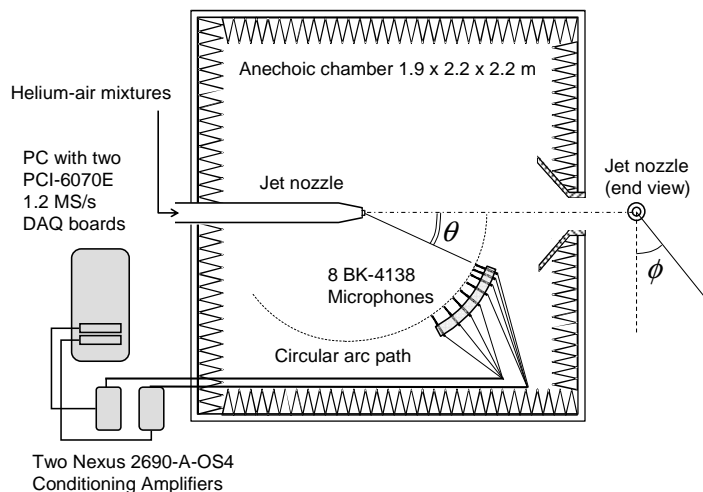


Figure 1 U.C. Irvine jet aeroacoustics facility.

A limited number of mean flow investigations were conducted in duplicate jet rig using a rake of Pitot probes. Due to large run times, pure air supplied at room temperature was used instead of the helium-air mixtures used in the acoustic tests. The mean axial velocity in the jet plume was surveyed using a Pitot rake system consisting of five probes, spaced apart by 10 mm, with hypodermic 0.5-mm internal diameter tips. Mounted on a three-dimensional motorized traverse, the rake scanned the entire jet plume at axial increments of 25.4 mm from the nozzle exit, up to seven jet diameters from the nozzle exit. The velocity was computed from the Pitot measurements under the assumptions of constant static pressure (equal to ambient pressure) and constant total temperature (equal to room temperature). Smoothing of

the velocity profiles was performed using a Savitzky-Golay filter.

Surveys for the baseline and beveled nozzle started at the nozzle exit plane ($x/D=0$). For the plug nozzles, because the plug would interfere with the motion of the Pitot rake, the surveys started downstream of the plug top ($x/D=2.4$).

The calculation of Perceived Noise Level (PNL) and Effective Perceived Noise Level (EPNL) was based on the following: flyover altitude of 1783 ft; engine diameter of 37.4 in.; zero angle of attack; and zero climb angle. Details of the PNL and EPNL calculation procedure can be found in Papamoschou⁴.

III. Nozzle configurations

The baseline case is a convergent round nozzle, tested at a nozzle pressure ratio (NPR) of 1.94 and used as a reference for comparing different configurations. It is representative of subsonic applications for which there is a significant existing database of both sub-scale acoustic tests and full scale certification FAR36 flight tests.

Nozzles of the external surface expansion type are desirable for supersonic applications as they can provide high thrust efficiencies over a wide range of pressure ratios without requiring variable geometries. The first modified

plume design was a beveled nozzle (Figure 2), originally thought to potentially improve noise directivity and take some advantage of shielding from the expansion ramp for sideline noise. This beveled nozzle was designed to work in a highly integrated manner with the airframe's fuselage. It is a three-dimensionally curved Single Expansion Ramp "SERN" type that can be thought of as an "inside out" plug where the extended tail surface of the nozzle is equivalent to the plug and was tailored for supersonic cruise pressure ratios greater than 5 (Figure 3). The potential noise benefit of beveled nozzles had been previously examined by Viswanathan⁵.



Figure 2 Left: Beveled nozzle model. Right: Rear view of integrated bevel nozzle design.

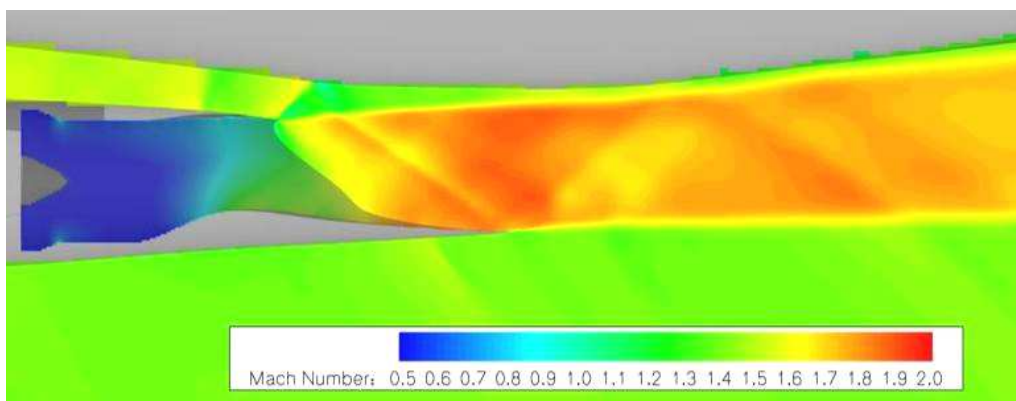


Figure 3 CFD of integrated beveled nozzle at supersonic speed

Several high radius plug (HRP) nozzles were also considered. Previous noise tests have shown an improvement using HRP nozzles, as described by Bauer, Kibens and Wleizen⁶. Porous plugs proved to be effective in reducing screech noise when shock cells were present.

A family of HRP nozzles was tested, including axisymmetric and non-symmetric plugs. A list of geometries tested is presented in Table 1. These nozzles were designed primarily to reduce noise, and performance, though always in mind, came second as a priority.

All the nozzles tested had an equivalent (area-based) diameter of 0.89 in. (22.6 mm). In the acoustic tests the nozzles were operated at NPR=1.94 using helium-air mixtures; the fully-expanded Mach number and velocity were 1.02 and 437 m/s, respectively. The mean-flow tests (using pure air supplied at room temperature) were conducted at slightly lower Mach number of 0.9 and velocity of 280 m/s.

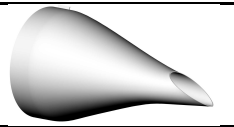
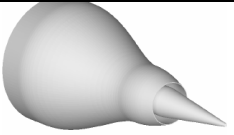
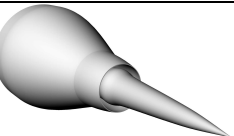
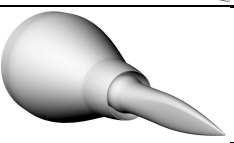
Bevel BV1.3 (Patented)		AEX503 ($\phi = 60$ deg) AEX506 ($\phi = 150$ deg) AEX509 ($\phi = 240$ deg)
High Radius Short Plug HRP1.1		AEX201 ($\phi = 0$ deg)
High Radius Long Plug HRP1.2		AEX601 ($\phi = 0$ deg)
High Radius Shaped Plug HRP1.3 (Patented)		AEX703 ($\phi = 60$ deg) AEX706 ($\phi = 150$ deg) AEX709 ($\phi = 240$ deg)

Table 1 Different nozzle configurations and azimuthal angles surveyed.

IV. Results

Results will be presented in the form of acoustic summaries showing narrowband sound pressure level (SPL) spectra in several polar directions; directivity of OASPL; PNL versus time and observer polar angle; and estimate of EPNL. Results for the baseline geometry are shown in Figure 4. Reference noise levels were thus established. For the deltas of EPNL and OASPL the improvement on noise level is shown in green, increase in noise level in red. On the spectra plots the red line will correspond to the reference case, “AEX101”, with the exception of the results on Figure 4.

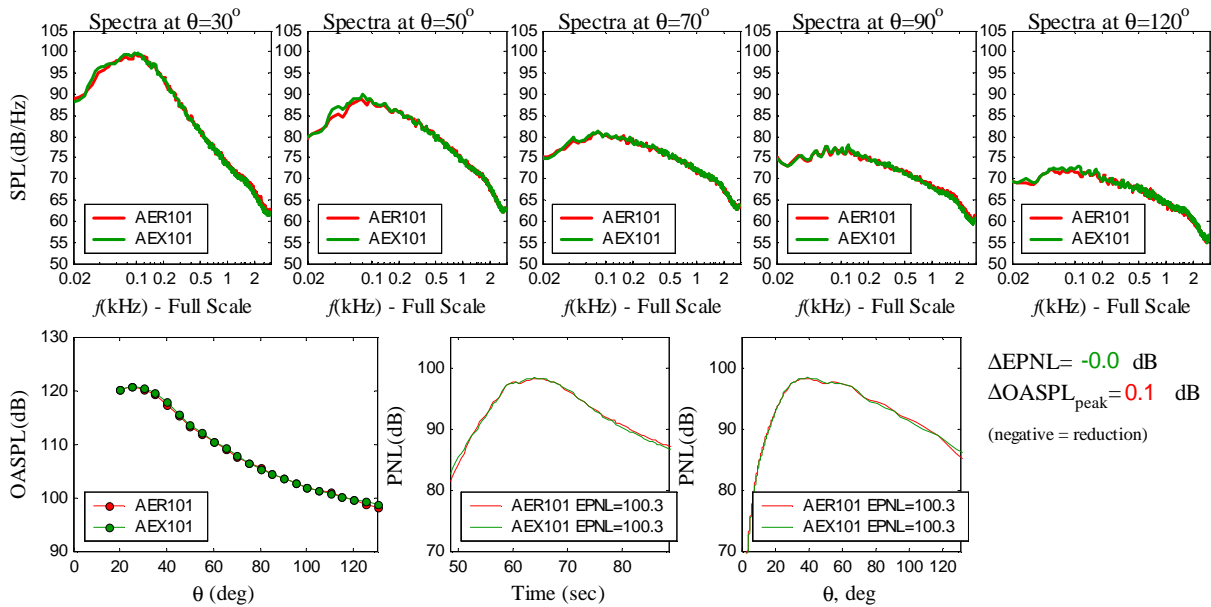


Figure 4 Noise levels for baseline. The red and green lines indicate repeat runs.

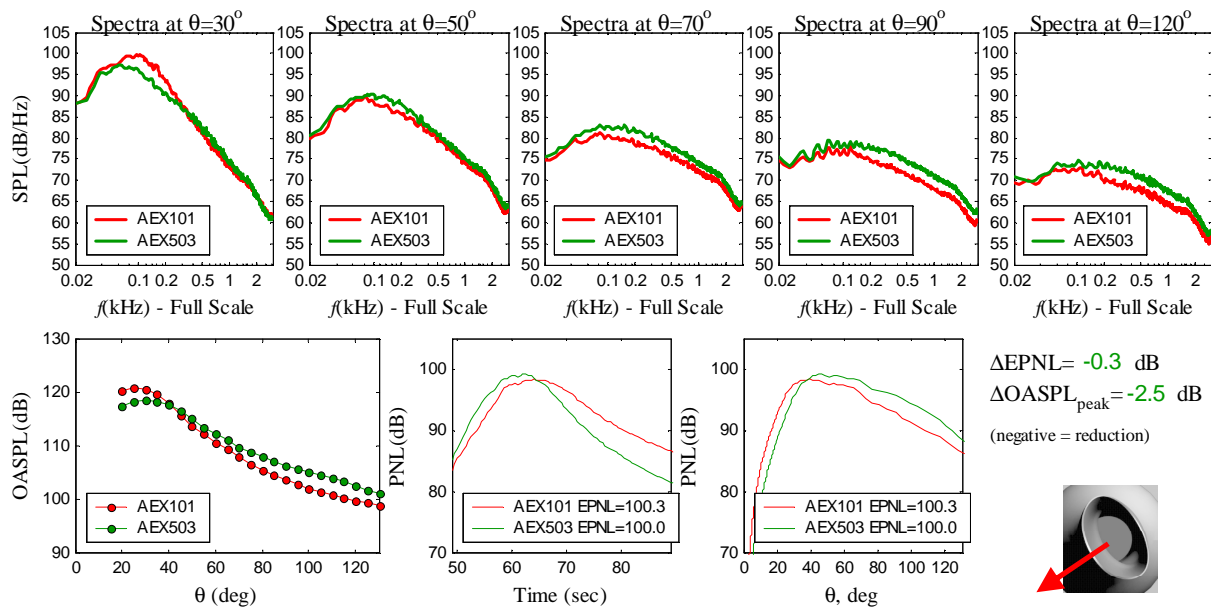


Figure 5 SPL, OASPL, and EPNL results at $\phi=60^\circ$ for BV1.3 (green lines) compared to baseline (red lines).

The beveled nozzle BV1.3 showed an improvement of 0.3 dB in EPNL and 2.5 dB in OASPL over the baseline nozzle for the 60° azimuth angle. Greater improvement was seen for $\phi=240^\circ$ with reductions in EPNL of 1.3 dB and 1.9 dB in OASPL (Figure 5 and Figure 7). Surveys at $\phi=150^\circ$ on the other hand showed increased noise levels of 3.2 dB EPNL and 0.4 dB OASPL as can be observed in Figure 6.

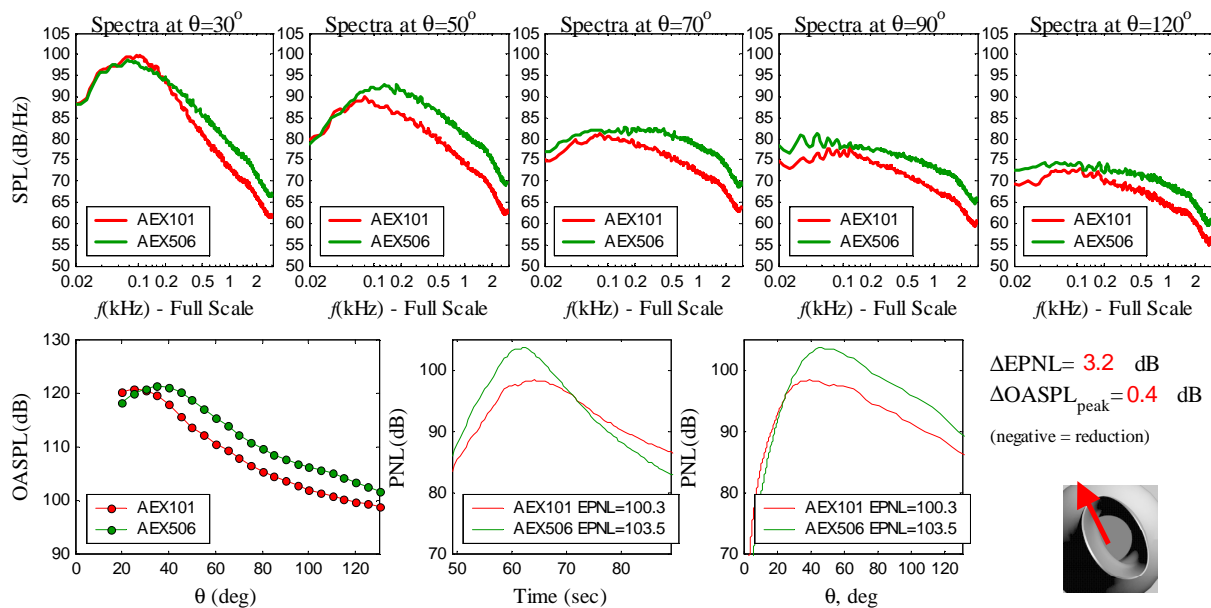


Figure 6 SPL, OASPL, and EPNL results at $\phi=150^\circ$ for BV1.3 (green lines) compared to baseline (red lines).

In contrast with previous bevel nozzle designs, BV1.3 is noisier at $\phi=150$ deg. This is consistent with the 90-deg rotation of the axes intended for this nozzle. The high SPL levels are accompanied with strong skewness of the time signal, indicative of enhanced Mach wave emission. (Papamoschou⁷)

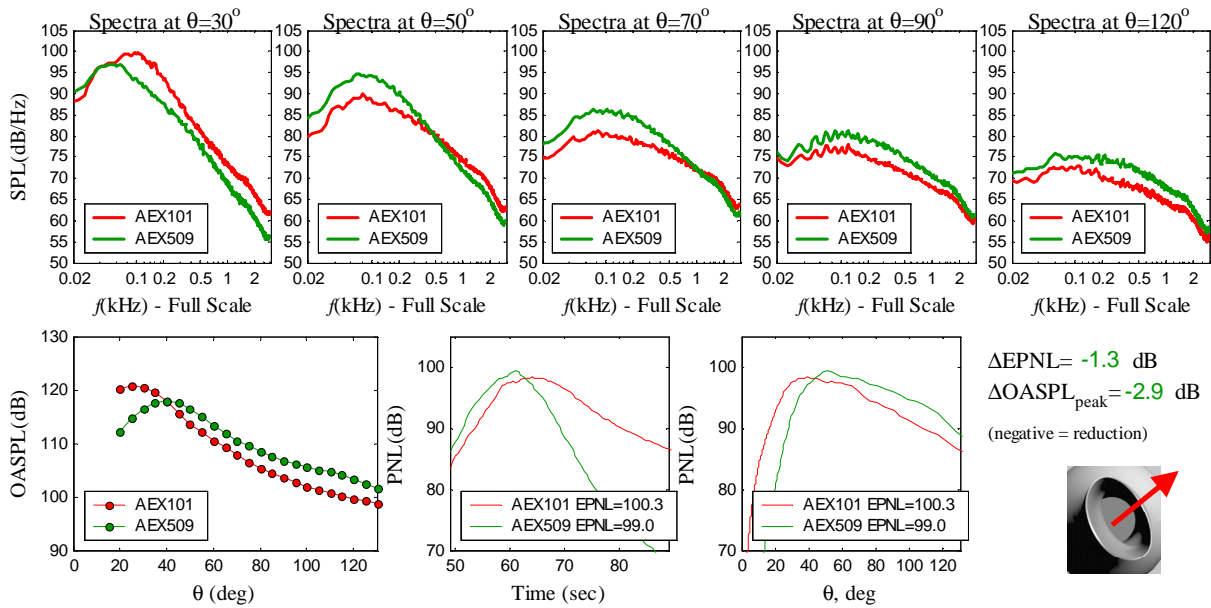


Figure 7 SPL, OASPL, and EPNL results at $\phi=240^\circ$ for BV1.3 (green lines) compared to baseline (red lines).

Flow field surveys of the beveled nozzle BV1.3 for a nozzle pressure ratio of 1.68 were performed at UCI and are presented in Figure 8 and Figure 9. Results show a flattening of the jet in agreement with the strong directivity of the noise. The shaping of the throat and not the beveling appears to be the reason for the flattening of the plume. The expansion ramp side of the bevel nozzle shapes the direction that the jet plume follows, shifting it away from the zero reference line ($y/D=0$).

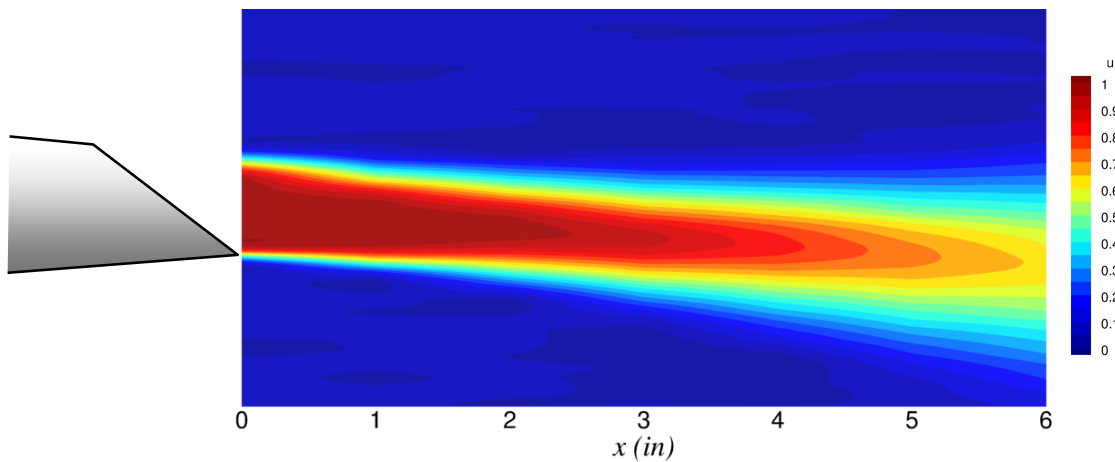


Figure 8 Contours of $u(x,y)/U_e$ for BV1.3.

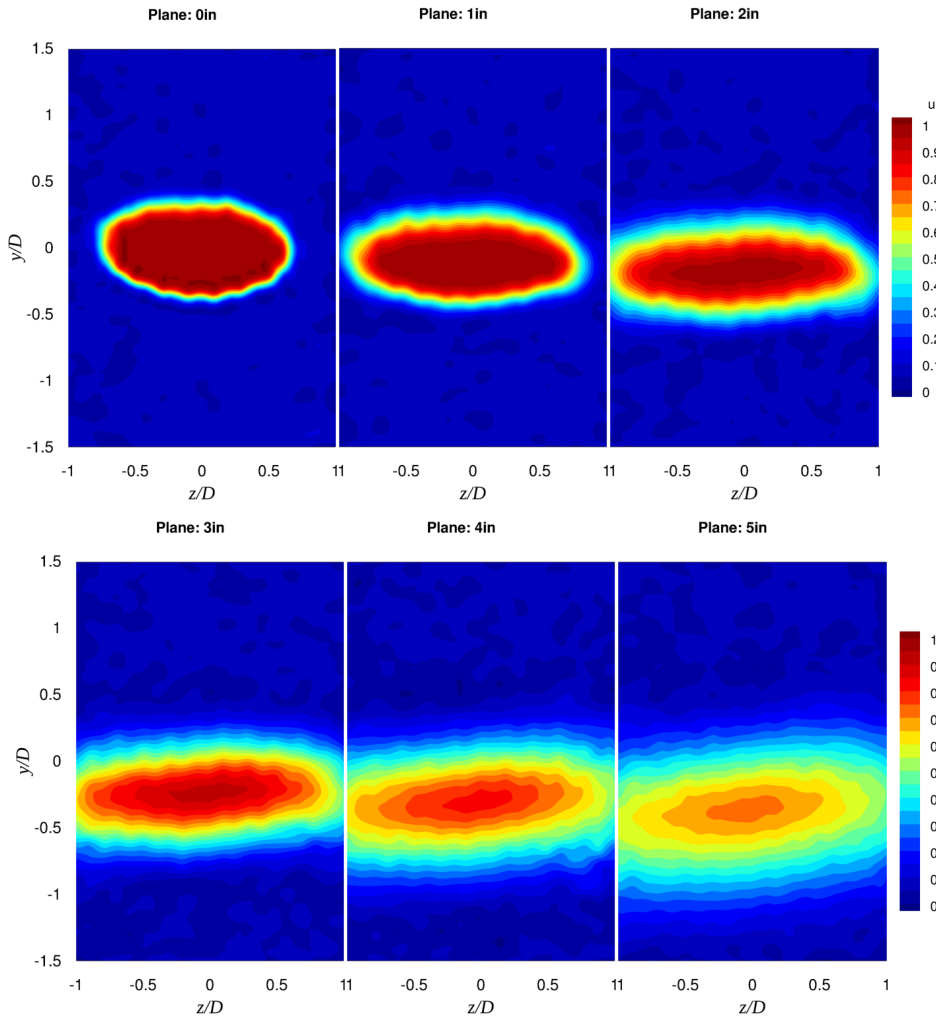


Figure 9 Flow survey: evolution of jet plume on beveled nozzle. Sections start at $x=0$ (exit plane), in increments of 1 inch. Contours of $u(y,z)/U_e$ for $NPR=1.68$.

The short radius plug nozzle –HRP1.1 (Figure 10)—had an overall reduction of 1.4 dB in EPNL and 1.4 dB in peak OASPL, as seen in Figure 11. The larger plug (HRP1.2 - Figure 10) more than doubled the noise reduction both in EPNL and OASPL, Figure 12.

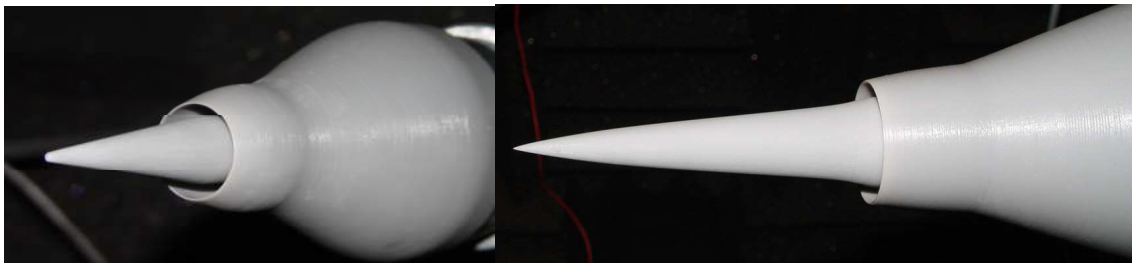


Figure 10 High radius plug nozzles. Left: short plug HRP1.1; right: long plug HRP1.2.

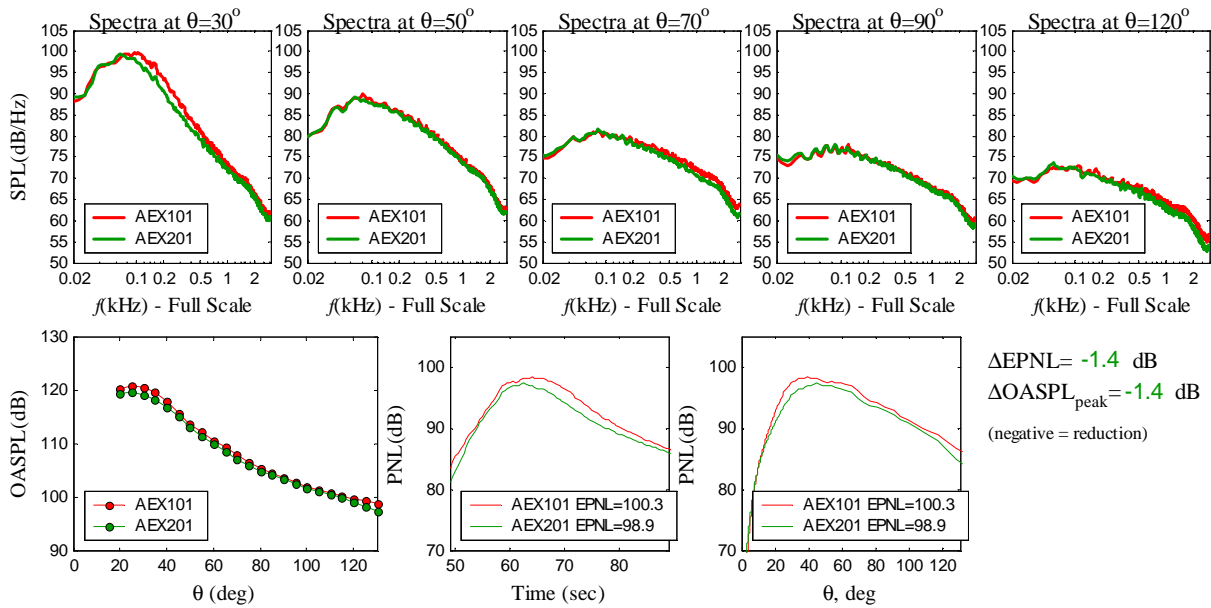


Figure 11 SPL, OASPL, and PNL results for HRP1.1 (green lines) compared to baseline (red lines).

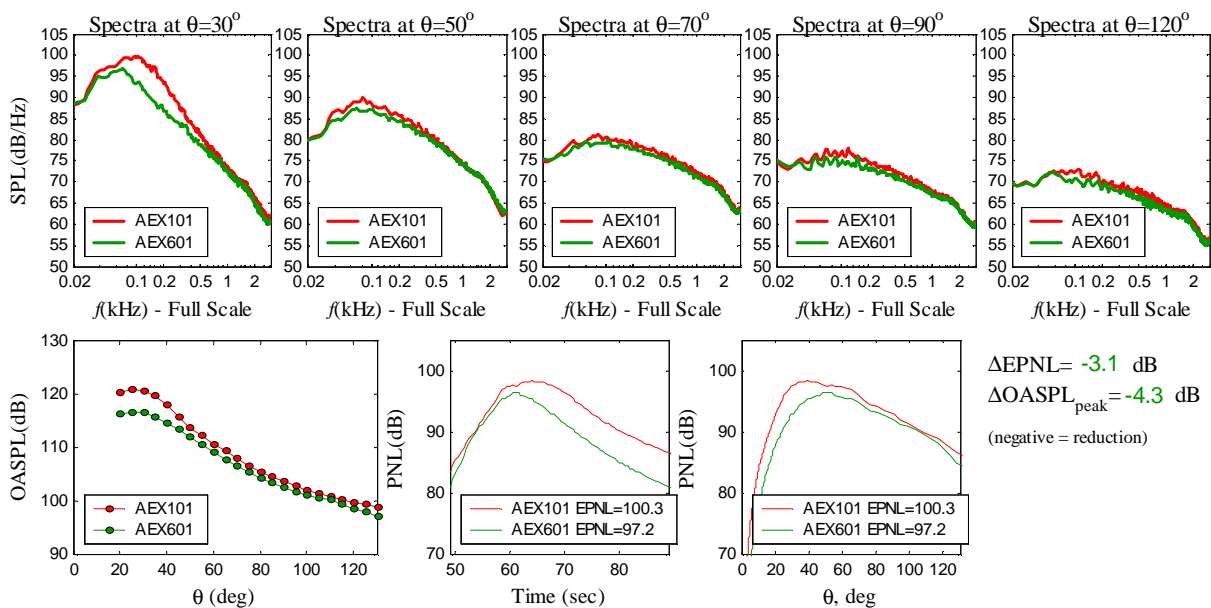


Figure 12 SPL, OASPL, and PNL results for HRP1.2 (green lines) compared to baseline (red lines).

Flow surveys of the high radius plug nozzle HRP1.2 are presented in Figure 13 and will be compared with computational predictions in Section V.

Finally, the shaped plug nozzle (HRP1.3, shown in Figure 14) was tested at azimuth angles $\phi = 60^\circ, 150^\circ$ and 240° (Figure 15 to Figure 17). HRP1.3 had the highest levels for noise reduction of the configurations tested, with reductions between 3.4 dB and 4.6 dB in EPNL and between 4.5 dB and 6.6 dB in OASPL. Noise reduction was found on all three azimuthal directions. The mean-flow evolution of the plume of HRP1.3 is depicted in Fig. 18

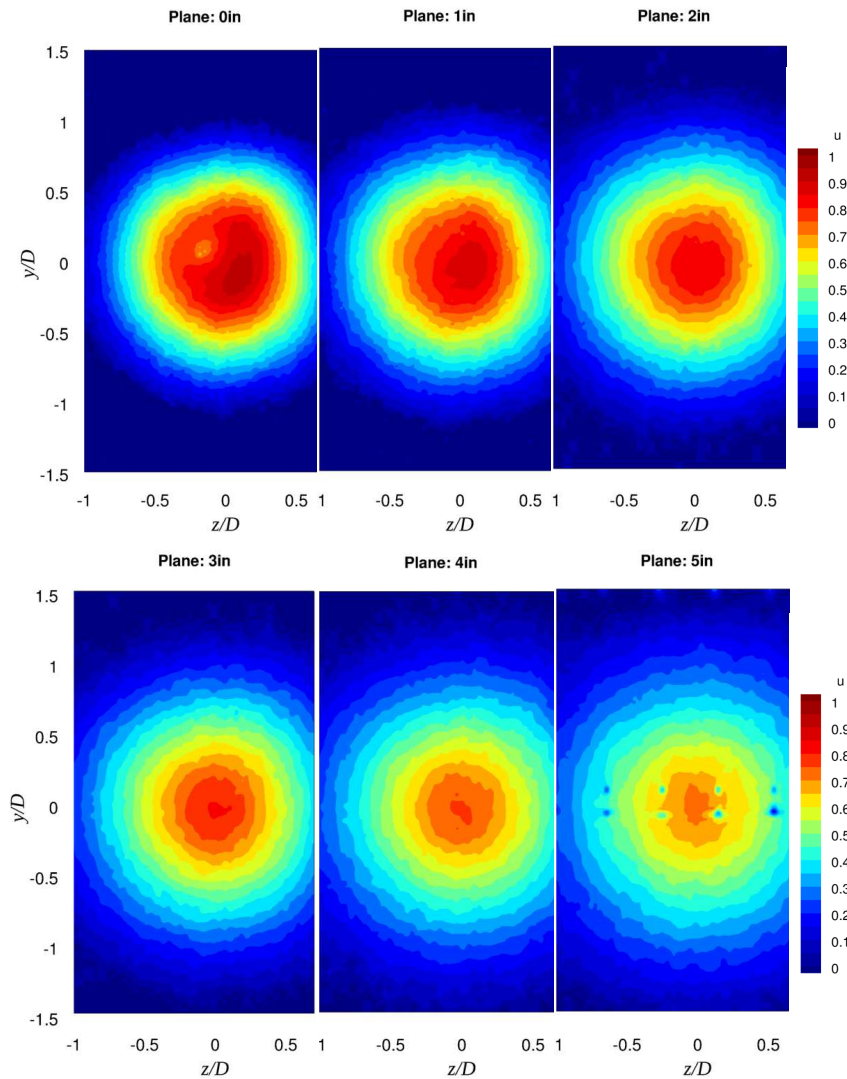


Figure 13 Flow survey: evolution of jet plume from HRP 1.2 plug nozzle. Sections start at $x=0$ (end of plug), in increments of 1 inch. Contours of $u(y,z)/U_e$ for $NPR=1.68$.



Figure 14 Shaped high radius plug nozzles (HRP1.3).

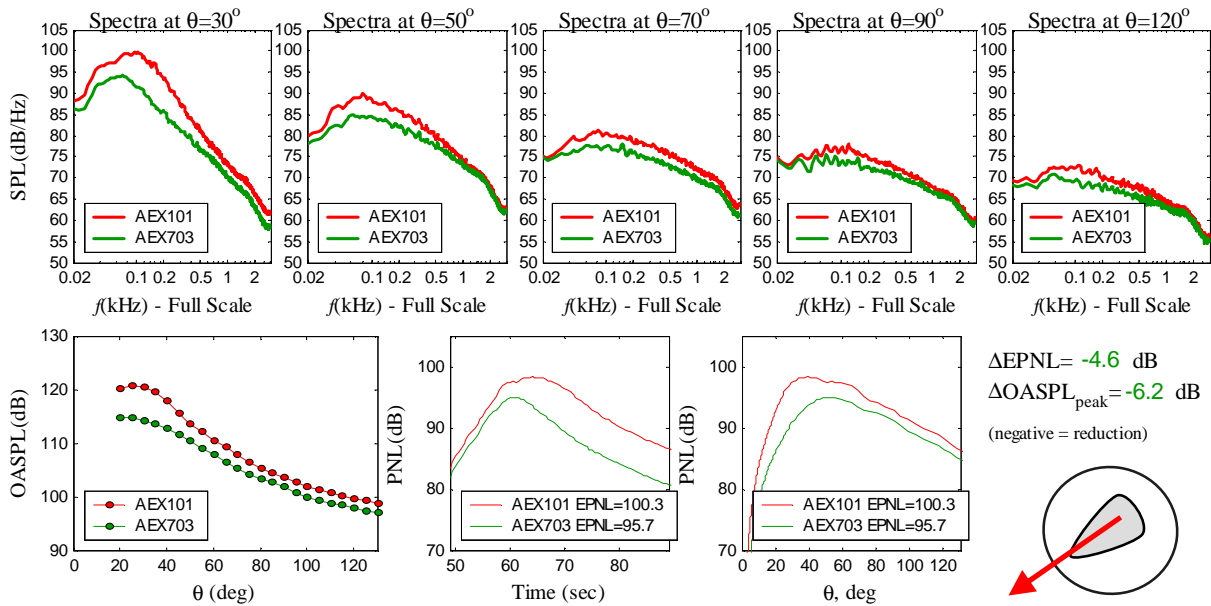


Figure 15 SPL, OASPL, and PNL results at $\phi=60^\circ$ for HRP1.3 (green lines) compared to baseline (red lines).

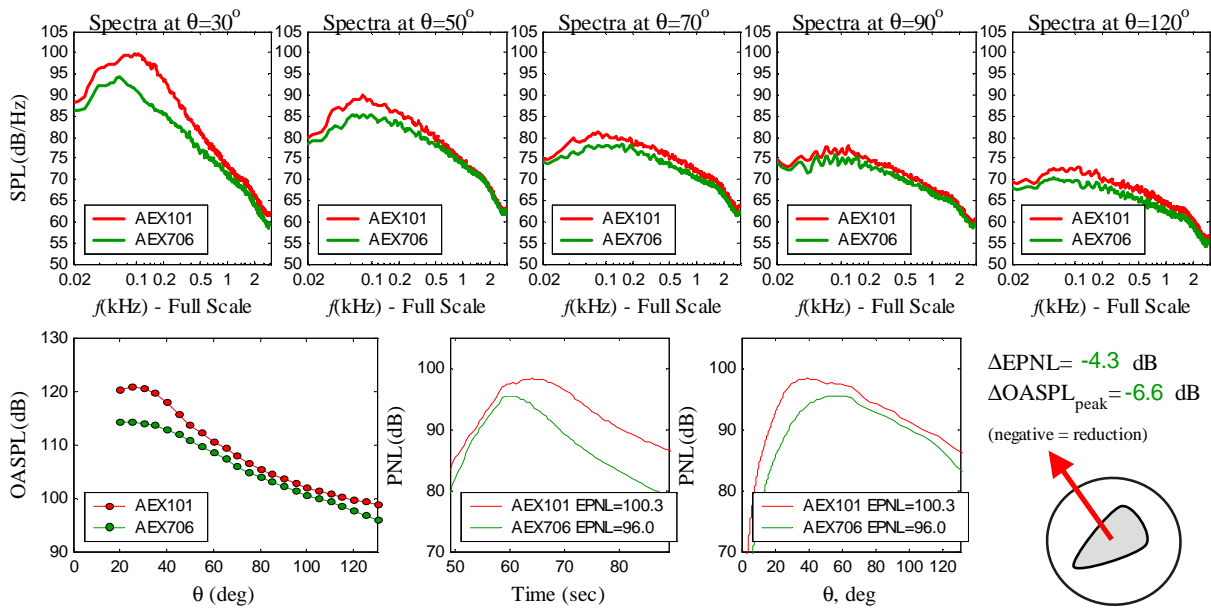


Figure 16 SPL, OASPL, and PNL results at $\phi=150^\circ$ for HRP1.3 (green lines) compared to baseline (red lines).

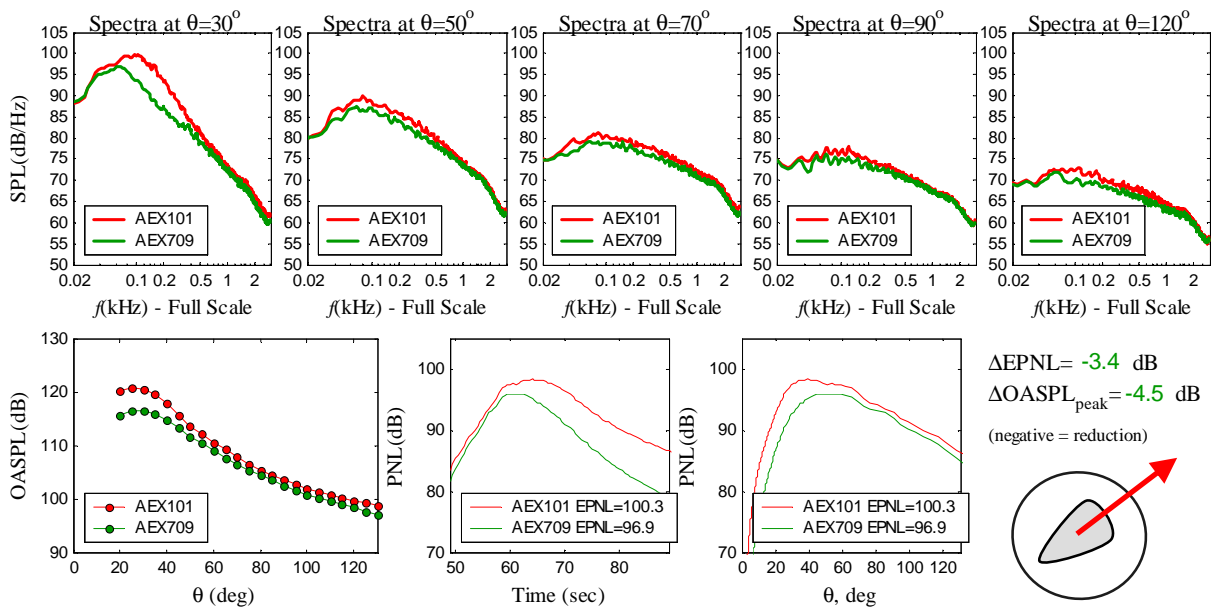


Figure 17 SPL, OASPL, and PNL results at $\phi=240^\circ$ for HRP1.3 (green lines) compared to baseline (red lines).

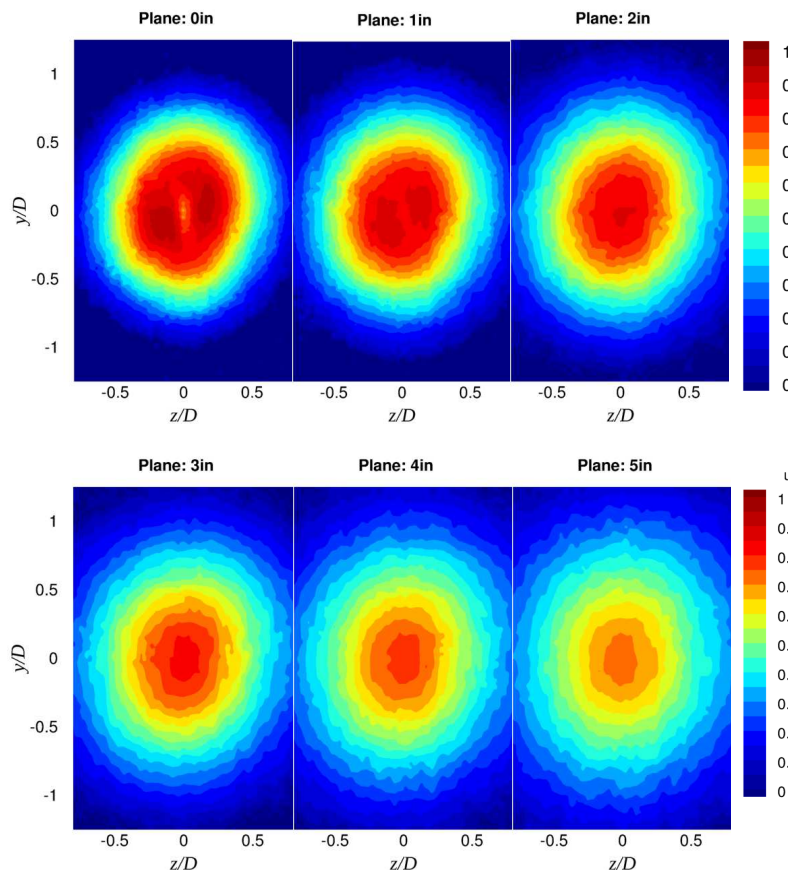


Figure 18 Flow survey: Evolution of jet plume on shaped plug HRP 1.3. Sections taken at $x=0$ (end of plug), in increments of 1 inch. Contours of $u(y,z)/U_e$ for $\text{NPR}=1.68$.

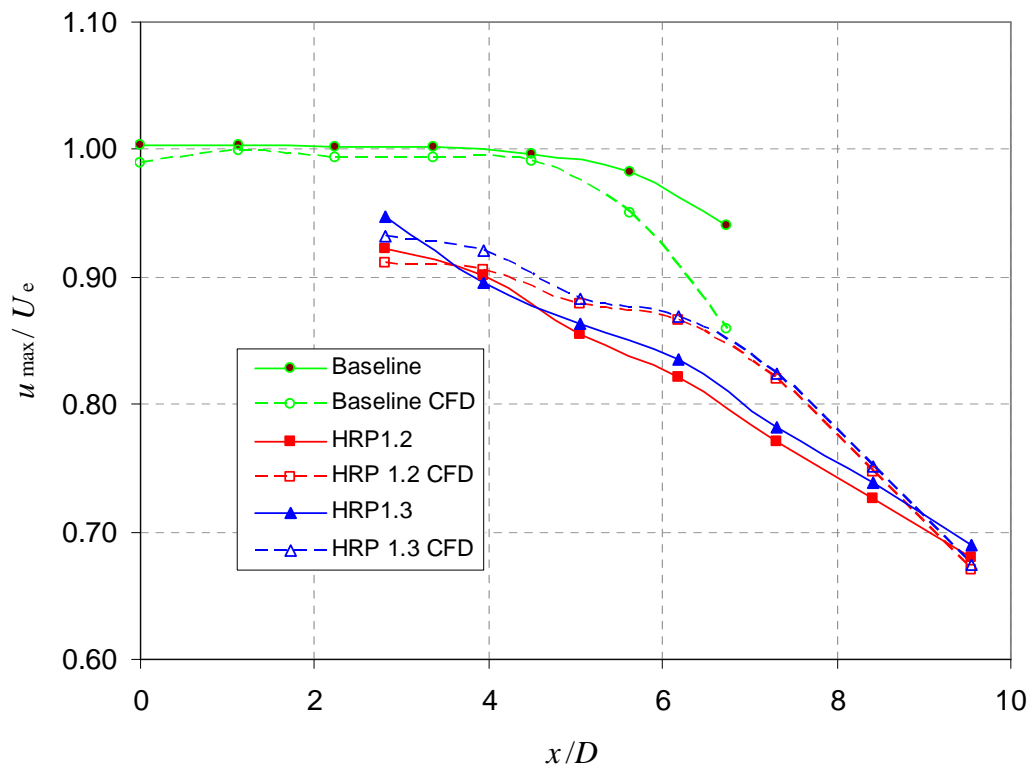


Figure 19 Axial decay of the local maximum of the mean velocity. Plot includes experimental measurements (solid lines) and numerical predictions (dashed lines) discussed in Section V.

The decay of the local maximum mean velocity with axial distance, plotted in Figure 19, offers some clues about the noise benefit of the plug nozzles. The plugs extended $2.4D$ downstream of the nozzle exit. Flow over the plug has suppressed level of turbulent kinetic energy because the plug surface restricts the turbulent velocity fluctuations. This, combined with the physical shielding of the plug, is expected to reduce noise considerably. Downstream of the plug ($x/D > 2.4$) we note a reduced mean velocity in comparison to the baseline nozzle at the same axial location. In addition, the velocity decay downstream of the plug is more rapid than for the baseline nozzle. The reduced velocity levels also contribute towards suppression of jet noise. No significant differences are seen between the HRP1.2 and 1.3 nozzle, so this general explanation cannot capture the additional benefit of the shaped plug nozzle.

V. Numerical Analysis

Computational Fluid Dynamics (CFD) analysis was done on some of the configurations using the **Fully-Unstructured Navier Stokes 3D** (FUN3D) code⁸⁻¹⁰. This code was originally developed by NASA's Langley Research Center as a research code in the early 1980's but has since grown to cover the incompressible, transonic, and hypersonic regimes and has been used on a wide variety of complex, large-scale problems. FUN3D solves steady and unsteady Euler and Reynolds-averaged Navier-Stokes (RANS) equations on node-based, mixed element grids for both incompressible and compressible flows. Due to the size of some of the problems being solved, FUN3D has the ability to decompose the domain and use message passage interface (MPI) communication for distributed computing, allowing for much short solve times.

The computational grids were created using Pointwise, a commercially available grid generation tool developed by Pointwise, Inc. Pointwise can create structured, unstructured, and hybrid grids and supports a wide variety of element types. These elements can collectively be composed into either 2-D or 3-D blocks depending on the user's needs. Grid generation is performed through a bottom-up approach, though changes to the grid propagate both forward and backward through the grid hierarchy, meaning the entire grid will be updated.

Several grids were used to determine a grid size such that results were independent of grid resolution. The final grid used had tetrahedral elements in the area contiguous to the plug with average cell size of 0.75 mm, $\sim 0.033D$. Different turbulent models were tried, including Spallart-Almaras^{11,12}, Menter SST^{11,13}, and Hybrid RANS-LES¹⁴. The Wilcox model produced the set of results closer to those obtained on the flow surveys. Results for the SST model were chosen over the other models after they were compared to the experimental data from the flow surveys. The data from the flow surveys corresponds to an average over a small fraction of time. Because of this, a RANS method was considered an appropriate option to use on the analysis.

The area of the plume has been studied to compare the results from the flow survey and the CFD solutions. The area was determined by computing only the region of the flow field with velocities greater than 0.3 ($u/U_e > 0.30$). A sample of the plumes sections and the computed areas are shown in Figure 20 to Figure 23.

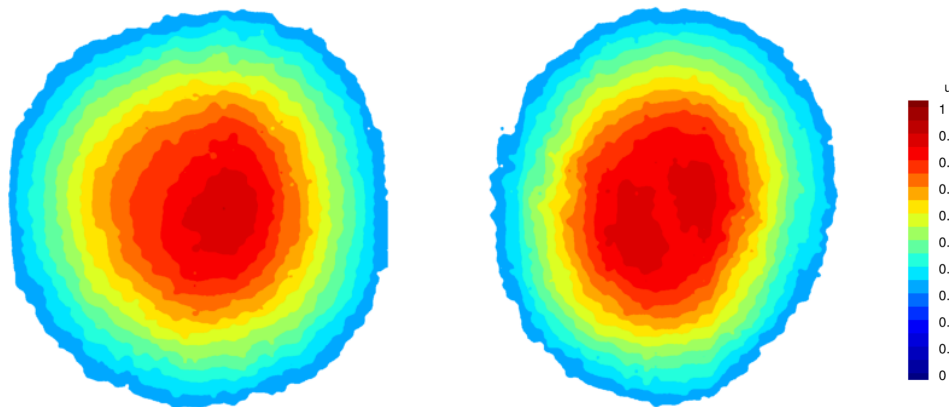


Figure 20 Plume shape for experiment at $x=1in$. Trimmed at $u/U_e=0.3$. Left, HRP1.2 (axisymmetric plug). Right, HRP1.3 (shaped plug).

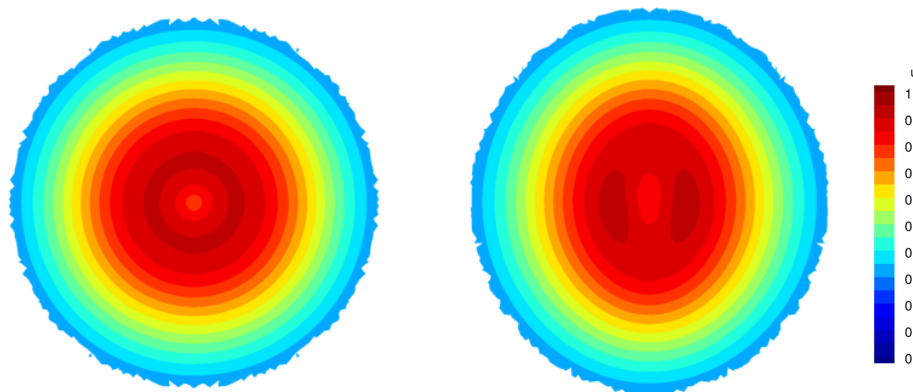


Figure 21 Plume shape for CFD at $x=1in$. Trimmed at $u/U_e=0.3$. Left, HRP1.2 (axisymmetric plug). Right, HRP1.3 (shaped plug).

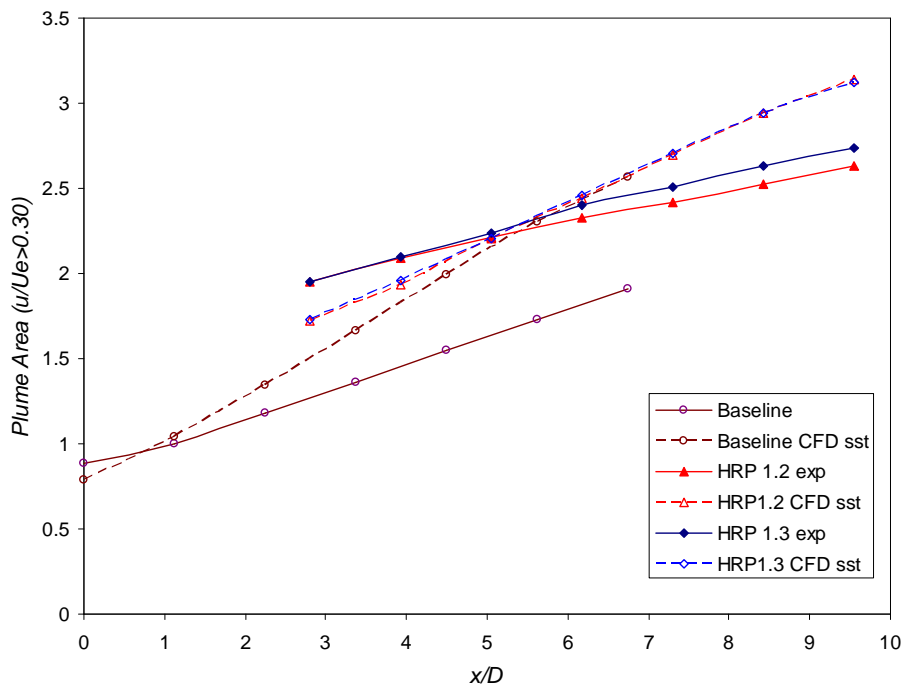


Figure 22 Plume evolution for plug nozzles. Experimental and computational results of plume area normalized by D^2

The slope for the evolution of the plume size as a function of distance on CFD solutions shows the numerical solution is expanding the jet at a greater rate than the experiment (Figure 22). Even though general agreement on flow topology is acceptable for the sections closer to the plug, as the plume moves away, the elliptic shape gives way to a more circular one.

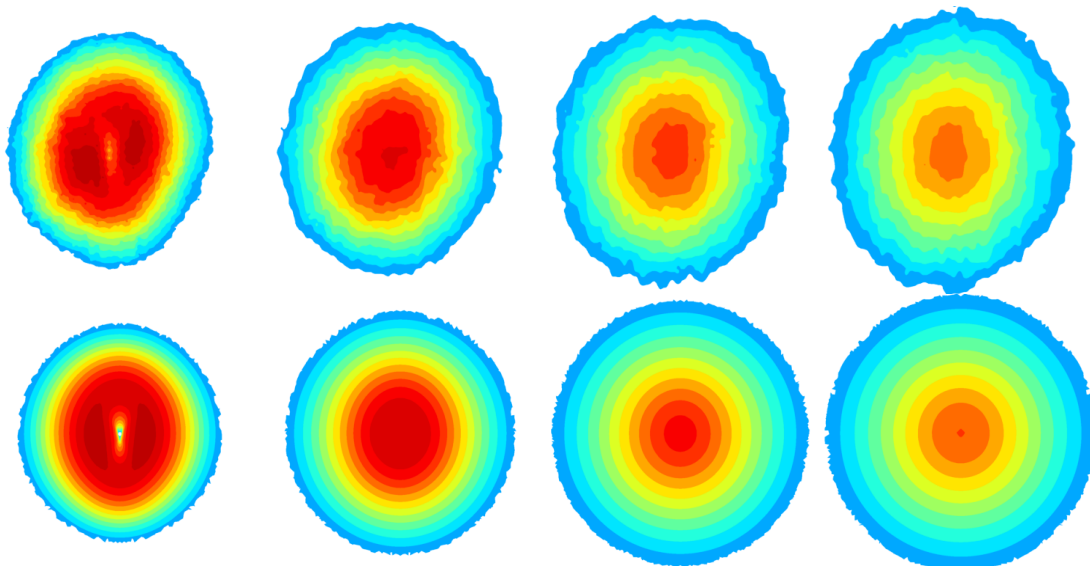


Figure 23 Comparison of plume shape for HRP1.3. Top: Experiment. Bottom CFD.

The trend on the decay of the local maximum mean velocity with axial distance from CFD data is consistent with the experimental results (Figure 19). The plug nozzles present an earlier drop in the maximum axial velocity, which

correlates to the evolution of momentum based on axial velocity on the plume, as can be seen in Figure 24. The momentum has been calculated using the normalized velocity (u/U_e) and a normalized density ρ/ρ_{inf} . The growth of the plume cross section accounts for the slight increase in computed momentum as it progresses downstream. The reduced momentum levels may also contribute towards suppression of jet noise. This may also be influenced by the viscous losses from skin friction on the plug's wetted area. A difference is now noticeable between the HRP1.2 and HRP 1.3 nozzles.

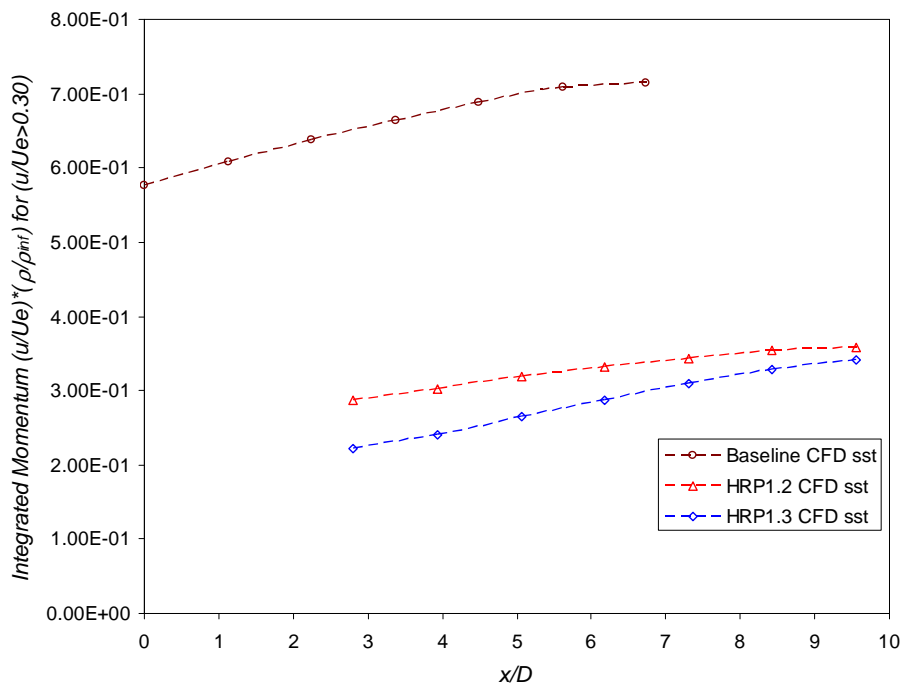


Figure 24 Evolution of plume momentum from CFD results

VI. Concluding Remarks

The exploration of beveled nozzles for the Aeron SSBJ was motivated by considerations of propulsion-airframe integration and the beneficial effects of beveled nozzles seen in past studies. However, the unique flow path of the Aeron beveled nozzles led to flow characteristics that generally increased, rather than reduced, the noise level. The principal flow feature responsible for the noise excess is thought to be the rapid distortion of the plume into a cross section with high aspect ratio, similar to an elliptical nozzle. Past research has shown that elliptical supersonic jets are generally noisier along the direction of the minor axis (Tesson, Petitjean and McLaughlin¹). This appears to be applicable to the jets produced by the Aeron nozzles, although in several instances the sound increased also along the major axis. The caution, therefore, is that simply the fact that a nozzle is beveled does not necessarily mean that it will be quieter. The complete flow path and resulting plume should be scrutinized. In addition, trends based on subsonic testing should not be expected to carry through to sonic or supersonic conditions.

The acoustics of the plug nozzles offered much greater promise for noise reduction. The larger the plug, the more substantial the noise reduction was. A likely reason for the benefit of the large plugs are the increased shear mixing area relative to jet depth promoting more rapid mixing with larger plug diameter and length, as well as shielding acoustically the noise sources in the part of the jet that is not in the line of sight of the observer. Additional aspects include suppression of turbulence levels due to the boundary condition imposed by the plug. Of course, the drawbacks include skin friction (thrust loss) because of the large wetted area and increased weight. The plug nozzle offers an interesting optimization problem of reducing noise while minimizing the thrust and weight penalty.

The improvements on noise levels for the shaped plug over the baseline were greater than those of the axisymmetric plug was puzzling. It was expected to see an improvement similar to that found on standard elliptic jets along the longer axis, but improvement was found all around. CFD results comparing both plug nozzles shed no light on the reason for this “all around” improvement, but did show a correlation between the momentum on the plume and noise reduction, suggesting the viscous losses on the plug may account for some of the noise reduction benefits.

References

- ¹ Tesson, X., Petitjean, B.P., and McLaughlin, K., “Experiments on the Noise Produced by High Speed Jets with Elliptic Exhaust Nozzles”, AIAA Paper 2005-0211, Jan 2005.
- ² Morris, P.J. and Bhat, T.R.S., “The Spatial Stability of Compressible Elliptic Jets,” *Physics of Fluids*, Vol.7, No.1, Jan. 1995, pp. 185-193.
- ³ Papamoschou, D., “Acoustic Simulation of Coaxial Hot Air Jets Using Cold Helium-Air Mixture Jets,” *Journal of Propulsion and Power*, Vol. 23, No. 2, 2007, pp. 375-381.
- ⁴ Papamoschou, D., “Fan Flow Deflection in Simulated Turbofan Exhaust,” *AIAA Journal*, Vol. 44, No.12, 2006, pp. 3088-3097
- ⁵ Viswanathan, K. 2004. Nozzle Shaping for Reduction of Jet Noise from Single Jets. *AIAA Journal*, Vol.43, No.5, May 2005, pp. 1008-1021.
- ⁶ Bauer, A.B.; Kibens, V., and Wlezien, R.W., “Jet noise suppression by porous plug nozzles”, NASA LaRC. Contractor Report 3613. Oct.1982
- ⁷ Papamoschou, D. and Debiassi M., "Directional Suppression of Noise from a High-Speed Jet," *AIAA Journal*, Vol. 39, No.3, 2001, pp. 380-387.
- ⁸ Anderson, W.K. and Bonhaus, D.L., “An Implicit Upwind Algorithm for Computing Turbulent Flows on Unstructured Grids,” *Computers & Fluids*, Vol. 23, 1994, pp. 1–22.
- ⁹ Anderson, W.K., Rausch, R.D., and Bonhaus, D.L., “Implicit/Multigrid Algorithms for Incompressible Turbulent Flows on Unstructured Grids,” *Journal of Computational Physics*, Vol. 128, 1996, pp. 391–408.
- ¹⁰ Nielsen, E.J., “Aerodynamic Design Sensitivities on an Unstructured Mesh Using the Navier-Stokes Equations and a Discrete Adjoint Formulation,” Ph.D thesis, Virginia Polytechnic Institute and State University, Blacksburg, VA, 1998.
- ¹¹ Rumsey, C.L., “Consistency, Verification, and Validation of Turbulence Models for Reynolds-Averaged Navier-Stokes Applications”, *3rd European Conference for Aerospace Sciences*. Versailles, France. 2009.
- ¹² Spalart, P. R., and Allmaras, S. R., “A One-Equation Turbulence Model for Aerodynamic Flows,” *Recherche Aerospaciale*, No. 1, 1994, pp. 5–21.
- ¹³ Menter, F. R., “Two-Equation Eddy-Viscosity Turbulence Models for Engineering Applications,” *AIAA Journal*, Vol. 32, No. 8, 1994, pp. 1598–1605
- ¹⁴ Lynch, C.E., Smith, M.J., “Hybrid RANS-LES Turbulence Models on Unstructured Grids”, AIAA Paper 2008-3854